Rock and Soil Mechanics

Volume 44 | Issue 2 Article 6

4-10-2023

An improved overload limit equilibrium method of rock blocks

Guo-feng XIAO
State Key Laboratory of Geomechanics and Geotechnical Engineering, Institute of Rock and Soil Mechanics, Chinese Academy of Sciences, Wuhan, Hubei 430071, China

Rock and Soil Mechanics 2023 44(2): 425−432 ISSN 1000−7598
https: //doi.org/10.16285/j.rsm.2022.5371 http://rocksoilmech.researchcommons.org/journal

An improved overload limit equilibrium method of rock blocks

XIAO Guo-feng

(State Key Laboratory of Geomechanics and Geotechnical Engineering, Institute of Rock and Soil Mechanics, Chinese Academy of Sciences, Wuhan, Hubei 430071, China)

Abstract: The lifting mode is one of the failure modes of finite movable blocks proposed by block theory. Although direct collapse is the most common failure mode in underground engineering, there is still a lack of suitable quantitative stability analysis methods, resulting in the scarcity of necessary theoretical support for the excavation and reinforcement design of underground engineering. To this end, an improved stability analysis method for rock blocks considering progressive damage is proposed. Main improvements include: introducing overload base and overload direction to quantify the reserve load; proposing two options of overload base which are Tan and Scal; and setting the overload direction on the boundary sector of the joint pyramid. The example verification results show that the improved method is fully compatible with the existing safety factor algorithm for the wedge failure mode. It realizes the quantitative stability analysis of the lifting mode. Finally, the stiffness assignment method and its sensitivity are discussed.

Keywords: block theory; rock mass stability analysis; rigid body limit equilibrium; embedded mode; overload safety factor; overload base; overload direction

1 Introduction

Stability analysis of rock masses, a prerequisite for geotechnical engineering design, can provide scientific guidance for the design of support structures[1]. Stability problems of rock masses involve many engineering fields such as mining engineering, road and bridge engineering, hydraulic engineering and construction engineering[2]. For current engineering applications, the limit equilibrium method is a mainly used method for quantitative stability analysis[1].

Based on the motion mode, the stability analysis methods of rock masses can be classified into two types: translational and rotational[3]. The translational stability analysis method was originally proposed by Wittke[4], John[5], and Londe et al.[6] based on the wedge-shaped body model, and the block theory proposed by Goodman et al.[7] extended it to arbitrary convex blocks. The concept of block theory is clear and its geometric theory is perfect, and it has been widely used in stability analysis and support design of rock engineering[8–9]. According to the active force direction, Shi [7, 10–11] classified movable blocks into four categories: lifting, single-face sliding, double- face sliding and embedded (stable even without friction).

For single-face sliding and double-face sliding, the safety factor algorithms have numerous forms[6, 12–13], which are compatible with each other. For the embedded mode, some scholars[8, 14] have also proposed safety factor algorithms. Zhang[14] used the block-dividing method, and Jiang et al.[8] used the vertical differential column method to discretize blocks with multiple discontinuity planes to conduct quantitative stability analysis. Both methods introduced the idea of the slice method in two-dimensional soil analysis, and the difficulties in the slice method were systematically analyzed by Zhu et al.[15] and Zheng[16]. For the lifting mode, Xiao et al.[17] introduced the description of intermittent coplanar discontinuities and achieved quantitative stability analysis by the tensile capacity of rock bridge. However, this method is not compatible with the conventional single/double-face sliding algorithms.

From the viewpoint of engineering, direct collapse is a common destabilization phenomenon in underground engineering, and a quantitative analysis method of the lifting mode is necessary. Only quantitative analysis can provide more reasonable technical support for excavation and reinforcement design.

Hence, this paper improves the stability analysis method considering progressive failure proposed by Xiao et al.[17]. The three main improvements are listed as follows: (1) introducing overload direction and overload base to quantitatively describe the reserve load; (2) restraining the overload direction on the boundary sector of the joint pyramid; and (3) proposing two ways of setting the overload base, i.e., Tan and Scale. The compatibility of the improved method with the traditional algorithm and its applicability to the lifting mode are verified by examples. Finally, the assignment problem of the stiffness parameter and its sensitivity are discussed.

2 Improved model and methodology

For convenience, the improved method is named overload limit equilibrium method considering progressive failure process (POLE) according to its main features, abbreviated as method. The POLE method consists of four parts: geometric model, mechanical model, static equilibrium and limit equilibrium.

2.1 Geometric model

A convex block is the intersection of finite negative half-spaces, represented algebraically as

Received: 25 March 2022 Accepted: 30 June 2022
Author: XIAO Guo-feng, male, born in 1975, PhD, Associate Professor, research interests: assessment and monitoring of stability of rock slopes.
E-mail: gfxiao@ whrsm.ac.cn

$$B=\bigcap_{i=1}^{m} H_i \tag{1}$$

where i is the serial number; m is the number of half-space; and H is the negative half-space.

The algebraic expression of the negative half-space is

$$H: \boldsymbol{n}\cdot\boldsymbol{x}\leqslant p \tag{2}$$

where p is the distance between origin and boundary plane; x is an arbitrary point in the negative half-space; $\boldsymbol{n}$ is the unit outward normal vector of the boundary plane, it can be written as

$$\boldsymbol{n}=\delta(\sin\alpha\sin\beta,\sin\alpha\cos\beta,\cos\alpha) \tag{3}$$

where δ is half space sign and with the two possible values: –1 or 1; α is the plane dip angle; and β is the plane dip direction.

The quantified description of a negative half-space requires 3 parameters: occurrence, half space sign and origin distance. The corresponding quantified description of a convex block requires 3 sets of parameters: occurrence sequence, half space sign sequence and origin distance sequence. The modeling algorithm is described in the Ref. [18].

2.2 Mechanical model

The mechanical model is shown in Fig. 1. The convex block is assumed to be a single rigid body and only translational motion is taken into account. The active force $\boldsymbol{F}_{\text{con}}$, also named the operating load, includes loads of definite magnitude and direction such as gravity, infiltration pressure, seismic force and reinforcement force. Only considering translational movement leads to simple vector summation for all loads.

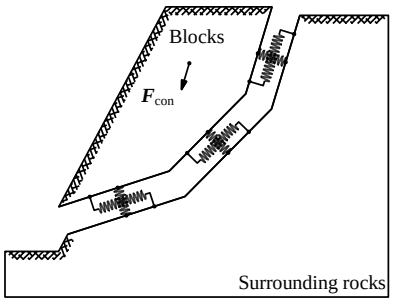

Fig. 1 Mechanical model for the static equilibrium analysis

Slip fracture planes, the physical contact interfaces between the block and the surrounding rocks, are enclosed by discontinuities. Described as intermittent coplanar discontinuities, each structural plane is composed of two plane units: fracture and rock bridge. The unit area is allocated in the following way

$$\left.\begin{aligned} S_i^{\text{J}} &= K_i S_i \\ S_i^{\text{B}} &= (1-K_i)S_i \end{aligned}\right\} \tag{4}$$

where S_i is the polygon area; K_i is the connectivity rate; and superscripts J and B denote crack unit and rock bridge unit respectively (same below).

Both the fracture unit and the rock bridge unit employ Goodman units to describe the relationship between stress and relative displacement, i.e.

$$\left.\begin{aligned} \boldsymbol{\sigma} &= k_{\text{n}}\boldsymbol{\varepsilon} \\ \boldsymbol{\tau} &= k_{\text{s}}\boldsymbol{\gamma} \end{aligned}\right\} \tag{5}$$

where $\boldsymbol{\sigma}$ and $\boldsymbol{\tau}$ are the normal and tangential stresses of the plane unit, and the direction of the normal stress vector is specified as the direction of the unit outer normal vector of the boundary plane; k_{n} and k_{s} are the normal and tangential stiffnesses (MPa/cm); and $\boldsymbol{\varepsilon}$ and $\boldsymbol{\gamma}$ are the normal and tangential relative displacements (cm).

Based on the assumption of rigid body translational motion, the relative displacement and the block displacement $\boldsymbol{u}$ of an arbitrary plane unit meet the geometric conditions:

$$\left.\begin{aligned} \boldsymbol{\varepsilon} &= (\boldsymbol{n}\otimes\boldsymbol{n})\boldsymbol{u} \\ \boldsymbol{\gamma} &= (\boldsymbol{E}-\boldsymbol{n}\otimes\boldsymbol{n})\boldsymbol{u} \end{aligned}\right\} \tag{6}$$

where $\boldsymbol{E}$ is the unit matrix; and $\otimes$ is the dyadic product.

The block is under the static conditions, the stress of the plane unit and the external force of the block satisfy the equilibrium conditions:

$$\sum_i\left[(\boldsymbol{\sigma}_i^{\text{B}}+\boldsymbol{\tau}_i^{\text{B}})S_i^{B}+(\boldsymbol{\sigma}_i^{\text{J}}+\boldsymbol{\tau}_i^{\text{J}})S_i^{\text{J}}\right]=\boldsymbol{F}_{\text{con}} \tag{7}$$

where i is the serial number of discontinuities.

2.3 Static equilibrium

Static equilibrium analysis is aimed at constructing a balanced stress field that satisfies both the static and strength requirements. The calculation is an iterative process (Fig. 2), which mainly contains four parts: block displacement, unit stress, failure determination and progressive failure. The block state is output after the computation cycles.

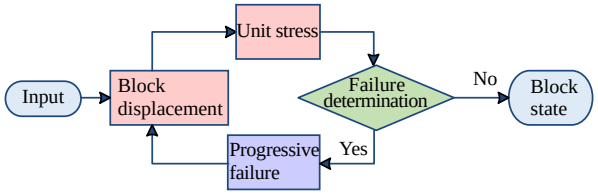

Fig. 2 Loop for calculating the static equilibrium

By substituting Eq.(6) into Eq.(5), the equations for obtaining the stresses of rock bridge unit and crack unit are derived as

$$\left.\begin{aligned} \boldsymbol{\sigma}_i &= k_{\text{n}i}(\boldsymbol{n}_i\otimes\boldsymbol{n}_i)\boldsymbol{u} \\ \boldsymbol{\tau}_i &= k_{\text{s}i}(\boldsymbol{E}-\boldsymbol{n}_i\otimes\boldsymbol{n}_i)\boldsymbol{u} \end{aligned}\right\} \tag{8}$$

where $k_{\text{n}i}$ and $k_{\text{s}i}$ are the normal and tangential stiffnesses of the plane unit with the serial number of i, respectively. Substituting Eq.(8) into Eq.(7) yields the block displacement:

$$\boldsymbol{M}\boldsymbol{u} = \boldsymbol{F}_{\text{con}} \tag{9}$$

$$\begin{aligned}\boldsymbol{M} = &\sum_i \left[(k_{\text{n}i}^{\text{B}} - k_{\text{s}i}^{\text{B}})(\boldsymbol{n}_i \otimes \boldsymbol{n}_i) + k_{\text{s}i}^{\text{B}} \boldsymbol{E} \right](1-K_i)S_i + \\ &\sum_i \left[(k_{\text{n}i}^{\text{J}} - k_{\text{s}i}^{\text{J}})(\boldsymbol{n}_i \otimes \boldsymbol{n}_i) + k_{\text{s}i}^{\text{J}} \boldsymbol{E} \right] K_i S_i\end{aligned} \tag{10}$$

The failure determination uses the existing strength criterion. The determination process is explicit. If the plane unit is identified to failure, the progressive failure description is described using the parameter reduction method. If not, the progressive failure of this unit ends.

The progressive rupture of the rock-bridge unit is described by the reduction of connectivity rate:

$$K_i^{(t+1)} = K_i^{(t)} + 0.01(1 - K_i^{(0)}) \tag{11}$$

where superscripts (t) and $(t+1)$ are the iteration steps; and superscript (0) is the initial value.

The connectivity rate is progressively increased with the progressive rupture of the rock-bridge unit. Since the maximum value of the connectivity rate is 1, when it reaches 1, the reduction stops and the progressive failure of this unit ends.

The yielding of the fracture plane unit is described by the stiffness reduction. The specific equation is

$$\left.\begin{aligned} k_{\text{n}i}^{\text{J}(t+1)} &= k_{\text{n}i}^{\text{J}(t)} + 0.010 k_{\text{n}i}^{\text{J}(0)} \\ k_{\text{s}i}^{\text{J}(t+1)} &= k_{\text{s}i}^{\text{J}(t)} - 0.015 k_{\text{s}i}^{\text{J}(0)} \end{aligned}\right\} \tag{12}$$

With the progressive yielding of the fracture unit, the normal stiffness is progressively increased and the tangential stiffness is progressively decreased. Since the tangential stiffness is non-negative, the reduction stops and the progressive failure of this unit ends when the tangential stiffness reaches 0. When the progressive failure of all plane units ends, the static equilibrium analysis process ends.

The output of the static equilibrium analysis is the state of the block. Based on the assumption of rigid body translation, there are only two states for the block: at-rest or motion. In engineering practice, there are mainly three types of rock instability phenomena: significant overall movement of rock and soil masses; significant morphological changes at the free face such as cracking, staggering, bulging and sinking; and functional loss or even complete failure of the reinforced structure. Therefore, the static equilibrium analysis of the rigid body is the most simplified model of rock instability phenomena.

The block state is determined using two parameters describing progressive failure: the connectivity rate and the fracture tangential stiffness. If the connectivity rate of all discontinuities composing the slip crack surface reaches the maximum value of 1 and the tangential stiffness of all fracture units reaches the minimum value of 0, the block is in motion; otherwise it is at rest.

2.4 Limit equilibrium

The limit state is the critical state between the stationary state and the moving state, i.e., the limit equilibrium state. Only considering the active force, the block state obtained from the static equilibrium analysis may be stationary or in motion, and the possibility in the limit state is extremely low.

To push the block to the limit state, the overload method[19–20] is introduced. In the static equilibrium analysis, the reserve load $\boldsymbol{F}_{\text{sto}}$ is superimposed to the service load of Eq.(9).

$$\boldsymbol{M}\boldsymbol{u} = \boldsymbol{F}_{\text{con}} + \boldsymbol{F}_{\text{sto}} \tag{13}$$

$$\boldsymbol{F}_{\text{sto}} = \eta \boldsymbol{F}_{\text{bas}} \boldsymbol{e}_{\text{sto}} \tag{14}$$

The quantitative description of the reserve load consists of three parameters: the overload coefficient η, the overload base $\boldsymbol{F}_{\text{bas}}$ and the overload direction $\boldsymbol{e}_{\text{sto}}$. After setting $\boldsymbol{F}_{\text{bas}}$ and $\boldsymbol{e}_{\text{sto}}$, the limit equilibrium state of the block is found by iteration of the overload coefficient η. The overload factor corresponding to the limit equilibrium state is named the critical overload coefficient, denoted as η_{cri}. The relation between the safety factor of the block SF and the critical overload factor is algebraically simple.

$$\text{SF} = \eta_{\text{cri}} + 1 \tag{15}$$

For $\text{SF} = 1$, the block is in the limit equilibrium state. For $\text{SF} > 1$, the reserve load has a clear engineering significance, a safety reserve to avert instability when subjected to uncertain loads. For $\text{SF} < 1$, the block stability analysis is a prediction of rock mass stability. In other words, the block will destabilize once the critical plane is excavated.

From the perspective of iterative algorithm, the overload coefficient requires an initial value, so the concept of zero point of overload coefficient is introduced. Taking the static equilibrium of the block in the overload direction into consideration

$$\eta_0 F_{\text{bas}} \boldsymbol{e}_{\text{sto}} + (\boldsymbol{F}_{\text{con}} \cdot \boldsymbol{e}_{\text{sto}}) \boldsymbol{e}_{\text{sto}} = 0 \tag{16}$$

Then the zero point of the overload coefficient is expressed as

$$\eta_0 = -\frac{\boldsymbol{F}_{\text{con}} \cdot \boldsymbol{e}_{\text{sto}}}{F_{\text{bas}}} \tag{17}$$

The overload base provides two setting options. First is the Tan option which is defined as the magnitude of the projected component of the active force in the overload direction.

$$F_{\text{bas}} = \boldsymbol{F}_{\text{con}} \cdot \boldsymbol{e}_{\text{sto}} \tag{18}$$

Second is the Scal option, which is defined as the active force scalar.

$$F_{\text{bas}} = F_{\text{con}} \tag{19}$$

The overload base of the Scal option is the scalar directly transformed from the active force vector, which is independent of the overload direction. In contrast, the overload base of the Tan option is based on the overload direction, which is the magnitude of the tangential component of the active force vector in one of the boundary surfaces of the joint pyramid.

The overload direction is set in the direction with the smallest angle to the active force direction on the joint pyramid boundary, regardless the block motion mode, including single-face, double-face, embedded or lifting. The embedded pyramid is the pyramid enclosed by all angular edge vectors $\boldsymbol{e}_{ij}$, also the unit external normal vectors:

$$\boldsymbol{e}_{ij} \cdot \boldsymbol{x} \leqslant 0 \tag{20}$$

When the active force direction vector is located in or at the boundary plane of the embedded pyramid, the block is in an embedded mode. Under pure gravity, the embedded mode of the discontinuities intersecting with the free face are "inward" or horizontal. It should be clearly pointed out that, in line with the definition of joint pyramid in block theory, as a geometric area, the embedded pyramid also contains the boundary plane of the pyramid.

The setting of the overload direction is based on the block theory. Shi [11] proposed the principle of "the nearest direction" for the determination of the motion pattern and the setting of the motion direction. This principle can be specified as the following three rules: (1) the motion direction is inside the joint pyramid or at the boundary sector; (2) the angle between the motion direction and the active force direction is smaller than 90°; (3) the angle between the motion direction and the active force direction is minimum.

From the perspective of static analysis, the overload direction and the motion direction can be regarded as the same concept. The overload direction is set by modifying two rules 1 and 2. For rule 1, the overload direction is restrained on the boundary of the joint pyramid. For rule 2, the angle between the overload direction and active force direction can be larger than or equal to 90°. The improvement of rule 2 is for the stability analysis of the embedded mode, whose minimum angle between the active force and the boundary surface of the joint pyramid is larger than 90°. The improvement of rule 1 is for the stability analysis of the lifting mode, whose active force direction is inside the joint pyramid.

After improvement, an extreme case of the overload direction needs to be considered, i.e., its angle to active force is 0° or 180°. These extreme cases appear in the lifting mode. During limit equilibrium analysis, the resultant force of the active force and the reserve load is 0 at the zero point of the overload coefficient, i.e., the right side of Eq. (13) is 0.

$$\boldsymbol{F}_{\text{con}} + \eta_0 F_{\text{bas}} \cdot \boldsymbol{e}_{\text{sto}} = 0 \tag{21}$$

Its physical meaning is that the block is in a state of weightlessness or suspension. It is not the state of rest, nor the state of motion, which is out of the theoretical scope of limit equilibrium analysis. At this point, it is directly set to $\text{SF} = 0$.

Based on the implicit definition, the algorithm for the safety factor is an iterative process, which can be divided into 3 steps. First, the accuracy of the safety factor is set to ε and the iteration interval of the overload factor is set to $[-\eta_{\max},\ \eta_{\max}]$. While extending the stability analysis scope to the lifting mode, the corresponding value range of the safety factor is extended to negative values. Second, static equilibrium analysis is performed at the zero point of the overload factor η_0 to determine the block state. If the block is stationary, the iteration interval is $[\eta_0, \eta_{\max}]$, otherwise it is $[-\eta_{\max}, \eta_0]$. Finally, according to accuracy requirements, the critical overload factor η_{mcr} and the corresponding safety factor are calculated iteratively within the iteration interval using the bisection method.

3 Validation by examples

3.1 Example 1

This example, based on the physical model test of Kumsar et al.[21], contains six precast concrete wedge-shaped blocks with the serial number from TB1 to TB6. The geometric parameters are defined according to the safety factor formula (Kovari's formula) proposed by Kovari et al.[13].

$$\text{SF} = \frac{\cos\omega_1 + \cos\omega_2}{\sin\left(\omega_1 + \omega_2\right)} \frac{\tan\varphi}{\tan i_{\text{a}}} \tag{22}$$

where φ is the friction angle; i_{a} is the dip angle of the intersection edge, and the plane determined by two vectors of intersection edge and active force is P0; and ω_1 and ω_2 are the dihedral angles of the discontinuities J1 and J2 with the plane P0. The geometric parameters of the Kumsar model are listed in Table 1.

Table 1 Geometrical parameters of the Kumsar model[21]

Symbol	TB1	TB2	TB3	TB4	TB5	TB6
i_{a}	29	29	31	27	30	30
ω	56	51	45	36	30	23

The physical test used the tilt test method, which changes the angle i_{a} by model rotation to measure i_{a} at $\text{SF} = 1$ so as to verify the effectiveness of the double-face sliding safety factor algorithm. The POLE method using Tan overload base option is marked as POLET, and the POLE method using Scal overload base option is marked as POLES . There are three purposes of calculation: (1) verify that the consistency of the POLE method using Scal option with physical test results; (2) verify that the results of the POLE method using Tan option is consistent with that using the Kovari formula; and (3) compare the POLE method using Scal option and the Kovari formula.

The geometric model is shown in Fig.3. The occurrences of free planes S1 and S2 are set to 0°/180° and 90°/180°, respectively, and the occurrences of discontinuities can be recalculated by the geometric parameters in Table 1. The plane serial number is (S1, S2, J1, J2), the half space sign sequence is (1, 1, –1, –1), and the origin distance sequence is (0, 0, 0, 0, 1).

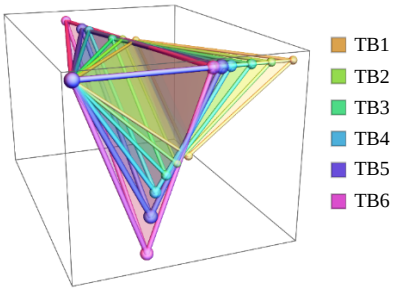

Fig. 3 Slip surface view of 3D geometrical model in Example 1

The normal and tangential stiffnesses are 1 000 and 1 MPa/mm, respectively, and the friction angles are 33°, 35° and 37°, respectively. The critical angle i_a is calculated by substituting $SF = 1$ into Eq.(22), and then the active force direction at the critical state are derived using i_a and occurrence of the plane P0. The calculation results show that the safety factors of 36 calculation schemes, including 6 models, 3 sets of friction angles and two overload base setting options (Tan and Scale), are all 1 (Fig. 4).

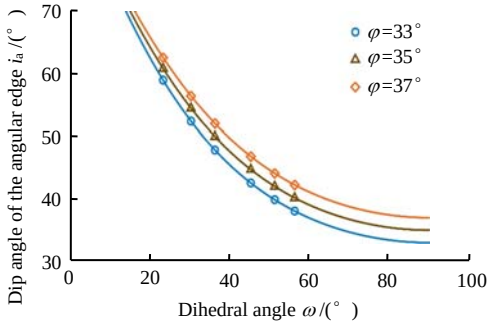

Fig. 4 Compatibility validation for SF=1

For $SF \neq 1$, 3 algorithms, including the POLE method using Tan option, the POLE method using Scal option and Kovari formula, are compared. The friction angle is set to 35°, and the interpolation of i_a is equidistant in the interval [0°, 90°] with a spacing of 10°. Models TB1 and TB6 are selected, and the calculation results are shown in Figs. 5 and 6. The curves of the POLE method using Tan option and the Kovari's formula are completely overlapped, which shows that it is fully compatible with the traditional double-face sliding algorithm.

There are two intersections for the curve obtained from the POLE method using Scal option with the Kovari curves, $SF = 0$ and $SF = 1$ (Figs. 5 and 6). For $0 < SF < 1$, the POLES curve is slightly higher than the Kovari curve. For $SF > 1$, the difference between the POLES curve and the Kovari curves is extremely significant. The safety factor of the POLES curve rises slowly as the dip angle of the angular edge decreases, and it is a constant when the dip angle of the angular edge is 0°. The safety factor of the Kovari curves rises rapidly as the dip angle of the angular edge decreases, and it is infinity for the dip angle of the angular edge decreases to 0°.

The Kovari formula is meaningless in engineering practice when the angle of inclination of the angular edge is 0°. For example, for a block placed on a horizontal plane, the safety factor using Kovari formula is infinity. Interpreted by overload, the block cannot be moved, no matter how large the external disturbance is. Although this extreme case is rare, slow dip slip plane <20° is common in practical engineering, and instability also frequently occurs. Therefore, the Kovari formula overestimates the stability state of rock masses under slow dip conditions. Compared with the Kovari formula, the POLE method using Scal option is of clearer engineering significance. The block is in a state of limit equilibrium when the disturbed load reaches (SF – 1) times the active force.

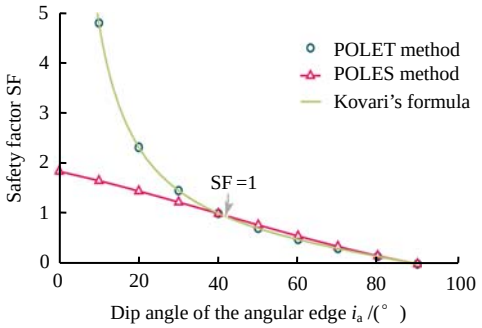

Fig. 5 Compatibility validation for SF≠1 (TB1)

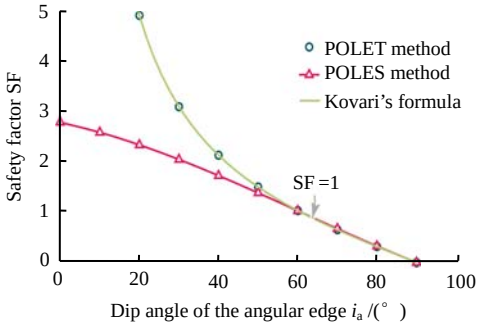

Fig. 6 Compatibility validation for SF≠1 (TB6)

3.2 Example 2

The example 2 is a tunnel located in the Alicante marble mine in southern Spain [22]. The cross-section of the tunnel is square with dimensions of 4 m×4 m, and the tunnel length is 20 m. The tunnel axis is at a strike of 180° and an inclination of 0° to 15°, with the rock weight of 25 kN/m^3. Menéndez-Díaz et al.[22] analyzed the block with the maximum volume within the cave roof, but the safety factor was not calculated.

Only the cave roof area was considered, and the planar occurrence and the strength parameters of discontinuities are listed in Table 2.

Table 2 Parameters of the free face and the discontinuities[22]

No. i	Dip angle α /(°)	Direction of dip β /(°)	Friction angle /(°)	Cohesion /kPa	Tensile strength /kPa
S1	0	0	—	—	—
J1	45	208	100	10	10
J2	48	133	50	10	5
J3	40	60	50	25	5
J4	70	335	100	25	10
J5	20	315	50	35	5
J6	10	205	100	35	10

According to block theory, a total of 111 finite movable blocks are identified, among which 20 are tetrahedra, 45 are pentahedra, 36 are hexahedra, and 10 are heptahedra. Herein a heptahedron (No. B105) is selected for geometric modeling. The modeling parameters include: the sequence of plane numbers (S1, J3, J4, J5, J1, J2, J6), the sequence of half space sign (–1, 1, –1, 1, 1, 1, 1); the sequence of origin distances (0, 0, 0, 2, 3.04, 0.22, 1.52). The geometric model of the block is presented in Fig. 7. The normal and tangential stiffnesses of the structural plane are set to 1 000 and 1 MPa/mm, respectively.

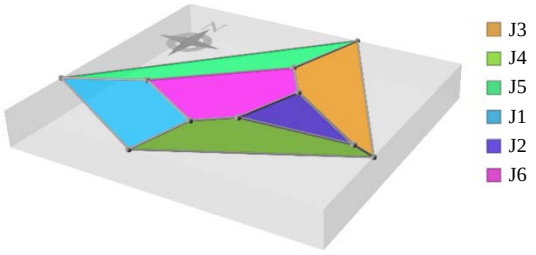

Fig. 7 3D geometrical model of Example 2

The safety factors using the POLE method using Tan option and the POLE method using Scal option are 0.995 1 and 0.995 4, respectively, as only gravity is considered for active force and the motion mode is J4 single-face sliding.

To verify the applicability of the POLE method for both embedded and lifting modes, the zenith angle along the direction of active force was interpolated at the interval of 2.5° within [0°, 180°]. The directional angle was set to 20°, and a total of 72 directions of active force were generated (Fig. 8). The block modes are embedded, J5J3 double-face sliding, J3 single-face sliding, lifting and J4 single-face sliding in order.

Menéndez-Díaz et al.[22] provided 3 parameters of the non-simplified MC damage criterion. The strength parameters are considered in three cases. For case MC1, both tensile strength and cohesion are 0 with a single-parameter form. For case MC2, tensile strength is 0 with the two-parameter simplified form. For case MC3, three parameters are not 0 with the complete MC criterion. Since the Tan mode is discontinuous at the interface of embedded and double-face sliding modes, only the Scal mode is considered for the overload base. There are a total of 219 calculation schemes.

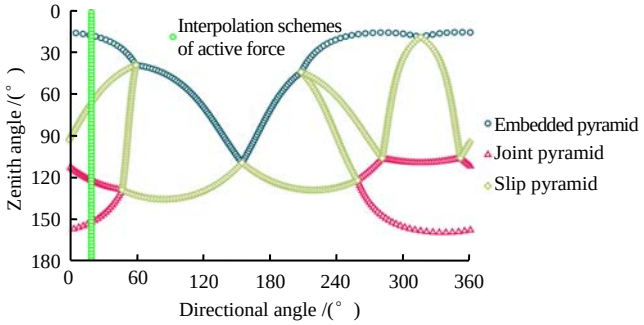

Fig. 8 Cylindrical projection of the active force interpolation scheme

The calculation results are displayed in Fig. 9. The quantitative stability analysis of the continuous transitions of the four modes in the full space along the active force direction were achieved using the POLE method. The motion modes experienced a total of 4 transitions.

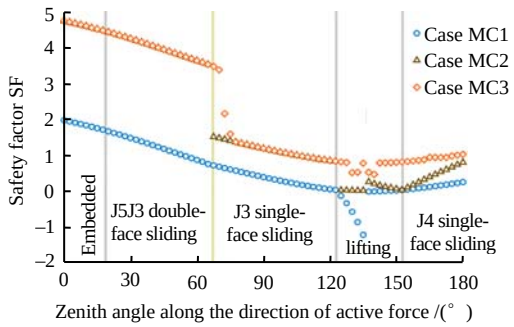

Fig. 9 Application verification of embedded and lifting modes

The first transition is from embedded mode to J5J3 double-face sliding mode. This two modes have the same overload direction which is the angular edge vector intersected by J5 and J3. The variation of the safety factor is also characterized by a smooth transition.

The second transition is from J5J3 double-face sliding to J3 single-face sliding. The transition of the safety factor under working condition MC1 is gradual, and the safety factor under working conditions MC2 and MC3 drops rapidly, indicating the high sensitivity of tensile strength and cohesion to the safety factor within this interval.

The third transition is a single-face sliding from J3 to lifting. The variation of the safety factor under working conditions MC1 and MC3 is continuous overall, but the safety factor under working condition MC2 drops. At the boundary point, SF is 0 for working conditions MC1 and MC2. During the lifting mode interval, a transition occurs for the overload direction (with the zenith angle of 136.25°), from the projection vector of the active force on the J3 plane to

that on the J4 plane, and the safety factor at this transition point jumps. The safety factor is most sensitive to strength parameters under the lifting mode. It can be inferred that safety factor is sensitive to block morphology if the direction of active force remains unchanged.

The fourth transition is a single-face sliding from lifting to J4. The change of safety factor is continuous until the active force direction is shifted to gravity direction (zenith angle is 180°).

The major difference between the Tan and Scal setting options for the overload base lies at the boundary point of the embedded to J5J3 double-face sliding mode, where the angle between the angular edge vector and the active force is 90°. Under the circumstances, the safety factor of the Tan mode is infinite. From the viewpoint of mechanics, the safety factor of the embedded mode is larger than the counterpart of the double-face sliding mode, so the Tan option cannot be extended to the embedded mode. The Scal option narrows the value domain of safety factor for $SF > 1$, thus making the quantitative stability analysis of the embedded mode feasible, which is one of the reasons for proposing the Scal setting method for overload base.

4 Discussions

Compared with the traditional algorithms, the stiffness parameter is added for the POLE method. There are two ways to obtain the stiffness parameter, i.e., experiments and empirical estimation. From the experimental viewpoint, the stiffness parameter test does not require a separate test, which can be obtained by monitoring the deformation data procedure during normal loading for the shear strength test of the structural plane. The test data processing can refer to that of elastic modulus. From the viewpoint of empirical data, the normal and the tangential stiffness intervals of the fracture is 110 to 1 690 MPa/mm and 50 to 1 200 MPa/mm, respectively. Some scholars[23–25] reviewed the current research status of empirical models.

In Sec. 3, the normal and tangential stiffnesses of the fracture are 1 000 and 1 MPa/mm, respectively, with the tangential to normal stiffness ratio (abbreviated as the stiffness ratio) of 0.001, which is significantly different from the empirical value of the Goodman unit. Therefore, two calculation schemes are designed based on the model condition of $SF = 1$ of example 1 to analyze the sensitivity of stiffness parameters to the POLE method using Tan option. In scheme 1 (S1), the stiffness ratio keeps constant at 0.001, and the normal stiffness is interpolated between 100 and 2 000 MPa/mm with at an interval of 100 MPa/mm. In scheme 2 (S2), the normal stiffness keeps constant at 1 000 MPa/mm, and the stiffness ratio is interpolated between 10^{-5} and 10^{0}. The iterative accuracy of the critical overload factor is set to 10^{-8}.

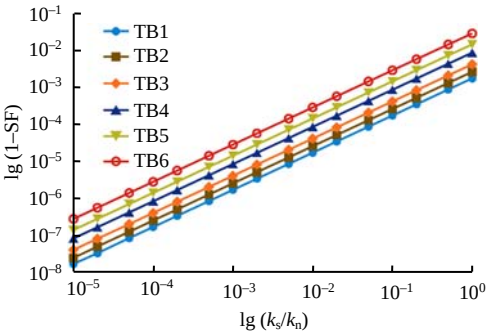

Fig. 10 Sensitivity analysis of the stiffness ratio

The results of S1 show that the safety factor is not affected by the normal stiffness under a constant stiffness ratio. The results of S2 (Fig. 10) show that the safety factor logarithmically decreases as the stiffness ratio increases, reaching the minimum value at the stiffness ratio of 1.The sensitivity of the stiffness ratio is related to the geometric model. When the stiffness ratio is 1, the effect on the TB1 model is minimal, with a reduction of safety factor by 0.001 8; and the effect on the TB6 model is maximal, with a reduction of safety factor by 0.028 4. As the stiffness ratio is 0.001, the difference between the safety factors by the POLE method using Tan option and by the Kovari formula is less than 10^{-5} orders of magnitude. To make the effect of stiffness parameters on the compatibility verification results less than 10^{-5} orders of magnitude, the normal and tangential stiffnesses of the fracture in Sec. 3 are 1 000 and 1 MPa/mm, respectively.

5 Conclusions

(1) In this paper, a stability evaluation method for blocks of the rocky slope is improved, named as the POLE method. The improved method inherits the main features of the original method, and the main improvement is the quantitative description method of the reserve load.

(2) The safety factor is defined using the overload reserve form. The overload base and the overload direction are introduced in the quantitative description of the reserve load. There are two setting options for the overload base, i.e., the Tan option and the Scal option. The overload direction is restrained on the boundary sector of the joint pyramid. Based on this restraint, the POLE method extends the applicability to the embedded and lifting modes.

(3) the POLE method using Tan option is completely compatible with the traditional double-face sliding mode. the POLE method using Scal option redefines the value domain of the safety factor and has a clearer engineering meaning.

References

[1] ZHENG Ying-ren, ZHAO Shang-yi. Application of strength reduction FEM in soil and rock slope[J]. Chinese Journal of Rock Mechanics and Engineering, 2004, 23(19): 3381–3388.

[2] LIU Li-ping, JIANG De-yi, ZHENG Shuo-cai, et al. The recent progress of the slope stability analysis methods[J]. Journal of Chongqing University (Natural Science), 2000, 23(3): 115–118.

[3] MAULDON M, GOODMAN RICHARD E. Vector analysis of keyblock rotations[J]. Journal of Geotechnical Engineering, 1996, 122(12): 976–987.

[4] WITTKE W W. Method to analyze the stability of rock slopes with and without additional loading[J]. Felsmechanick und Ingenieurgeolgie, 1965, 30(Suppl. II): 52–79.

[5] JOHN K W. Graphical stability analysis of slopes in jointed rock[J]. Journal of the Soil Mechanics and Foundations Division, 1968, 94(2): 497-526.

[6] LONDE P, VIGIE G, VORMERINGER R. Stability of rock slopes, a three-dimensional study[J]. Journal of the Soil Mechanics and Foundations Division, 1969, 95(1): 235–262.

[7] GOODMAN R E, SHI G. Block theory and its application to rock engineering[M]. Englewood Cliffs, New Jersey: Prentice-Hall, Inc., 1985: 338.

[8] JIANG Q H, ZHOU C B. A rigorous solution for the stability of polyhedral rock blocks[J]. Computers and Geotechnics, 2017, 90(10): 190–201.

[9] ZHANG Qi-hua, ZHANG Yu, LI Li-ping, et al. Advances in application of block theory to stability analysis of rock mass surrounding caverns[J]. Hazard Control in Tunnelling and Underground Engineering, 2020, 2(4): 9–18.

[10] SHI Gen-hua. Tereoprojection method of stability analysis of rock mass[J]. Science in China, 1977(3): 260–271.

[11] SHI Gen-hua. Geometrical approach of rock mass stability analysis[J]. Science in China, 1981(4): 487–495.

[12] HOEK E, BRAY J. Rock slope engineering[M]. 3rd ed. London: Institution of Mining and Metallurgy, 1981.

[13] KOVARI K, FRITZ P. Stability analysis of rock slopes for plane and wedge failure with the aid of a programmable pocket calculator[C]//The 16th US Symposium on Rock Mechanics. Minneapolis, Minnesota: [s. n.], 1975: 25–33.

[14] ZHANG Qi-hua. Block limit equilibrium analysis method for multi-sliding surface block[J]. Chinese Journal of Rock Mechanics and Engineering, 2007, 26(8): 1625–1632.

[15] ZHU Da-yong, QIAN Qi-hu. Rigorous and quasi-rigorous limit equilibrium solutions of 3D slope stability and application to engineering[J]. Chinese Journal of Rock Mechanics and Engineering, 2007, 26(8): 1513–1528.

[16] ZHENG Hong. A rigorous three-dimensional limit equilibrium method[J]. Chinese Journal of Rock Mechanics and Engineering, 2007, 26(8): 1529–1537.

[17] XIAO Guo-feng, CHEN Cong-xin. Simulation of progressive failure process and stability analysis method for rock block[J]. Rock and Soil Mechanics, 2018, 39(8): 3001–3010.

[18] XIAO Guo-feng, CHEN Cong-xin. An analytic method for geometrical construction of convex polyhedron block[J]. Rock and Soil Mechanics, 2017, 38(6): 1657–1665.

[19] ZHENG Ying-ren, ZHAO Shang-yi. Discussion on safety factors of slope and landslide engineering design[J]. Chinese Journal of Rock Mechanics and Engineering, 2006, 25(9): 1937–1940.

[20] ZHENG Hong, TIAN Bin, LIU De-fu, et al. On definitions of safety factor of slope stability analysis with finite element method[J]. Chinese Journal of Rock Mechanics and Engineering, 2005, 24(13): 2225–2230.

[21] KUMSAR H, AYDAN Ö, ULUSAY R. Dynamic and static stability assessment of rock slopes against wedge failures[J]. Rock Mechanics and Rock Engineering, 2000, 33(1): 31–51.

[22] MENÉNDEZ-DÍAZ A, GONZÁLEZ-PALACIO C, ÁLVAREZ-VIGIL A E, et al. Analysis of tetrahedral and pentahedral key blocks in underground excavations[J]. Computers and Geotechnics, 2009, 36(6): 1009–1023.

[23] JIANG X W, WAN L, WANG X S, et al. Estimation of fracture normal stiffness using a transmissivity-depth correlation[J]. International Journal of Rock Mechanics and Mining Sciences, 2009, 46(1): 51–58.

[24] SINGH R, PATHAK S. In-situ normal stiffness of rock mass[C]//4th Indian Rock Conference. Solan, Himachal Pradesh: [s. n.], 2013: 181–188.

[25] YAO C, SHAO J F, JIANG Q H, et al. Numerical study of excavation induced fractures using an extended rigid block spring method[J]. Computers and Geotechnics, 2017, 85(5): 368–383.